RSC Advances

ROYAL SOCIETY OF CHEMISTRY

www.rsc.org/advances

RSC Advances

ARTICLE

Influence of carbon nanomaterials defects on the formation of protein corona

Bishwambhar Sengupta,[a, b] Wren E. Gregory,[a, b] Jingyi Zhu,[a] Siva Dasetty,[c] Mehmet Karakaya,[a] Jared M. Brown,[d] Apparao M. Rao,[a, e] John K. Barrows,[f] Sapna Sarupria,[b*] and Ramakrishna Podila[a, b, e*]

Received 00th July 20xx,
Accepted 00th July 20xx

DOI: 10.1039/x0xx00000x

www.rsc.org/

Abstract: In any physiological media, carbon nanomaterials (CNM) strongly interact with biomolecules leading to the formation of biocorona, which subsequently dictates the physiological response and the fate of CNMs. Defects in CNMs play an important role not only in materials properties but also in the determination of how materials interact at the nano-bio interface. In this article, we probed the influence of defect-induced hydrophilicity on the biocorona formation using micro-Raman, photoluminescence, infrared spectroscopy, electrochemistry, and molecular dynamics simulations. Our results show that the interaction of proteins (albumin and fibrinogen) with CNMs is strongly influenced by charge-transfer between them, inducing protein unfolding which enhances conformational entropy and higher protein adsorption.

1. Introduction

The increased use of engineered nanomaterials (ENMs) in biomedicine has raised natural concerns regarding their adverse immune response.[1, 2] Blood is the first physiological environment that ENMs encounter upon intravenous injection for use as a drug delivery vector or a biomedical imaging contrast agent. Previously, it was shown that many different proteins and lipids compete between themselves for adsorbing on to the surface of ENMs to form a bio "corona".[3-5] Interactions between ENMs and the adsorbed proteins in the bio-corona may alter the structural arrangement of proteins leading to changes in their secondary structure through protein unfolding.[3-9]

The formation of biocorona and ensuing protein structural changes play an important role in complement initiation (through C3b protein) and adverse reactions of ENMs.[10, 11] A detailed understanding of the ENM-biomolecular interactions is therefore necessary to completely understand ENM toxicity and immune response.[12-15]

Among the wide variety of nanostructures, carbon nanomaterials (CNMs) represent an intriguing set of ENMs from biological and toxicity standpoints because CNMs: i) possess excellent affinity for proteins through hydrophobic and aromatic π–π stacking interactions, [16, 17] and ii) exhibit unique molecular charge-transfer among themselves and with other molecules including proteins. [18-20] For instance, C_{60} is known to display charge-transfer interactions with electron donor molecules including organic amines, [20] while graphene and single-walled carbon nanotubes (SWNTs) can act as either electron donors or acceptors with proteins such as streptavidin.[19] Indeed, charge transfer interactions between proteins and CNMs have previously been implicated in destabilizing adsorbed proteins/enzymes, which could in turn elicit adverse physiological response.[9, 21] While the root cause of ENM (particularly CNM) toxicity is still a subject of ongoing research, numerous studies have identified the presence of bioactive defects in ENMs (including Au, Ag, TiO_2, SiO_2, and CNMs) as

[a] Department of Physics and Astronomy, Clemson Nanomaterials Center, Clemson University, Clemson, South Carolina 29634, United States
[b] Laboratory of nano-biophysics, Clemson University, Clemson, South Carolina 29634, United States.
[c] Department of Chemical and Biomolecular Engineering, Clemson University, Clemson, South Carolina 29634, United States.
[d] Department of Pharmaceutical Sciences, Skaggs School of Pharmacy and Pharmaceutical Sciences, The University of Colorado Anschutz Medical Campus, Aurora, CO 80045, United States
[e] COMSET, Clemson University, Anderson, SC 29625, United States.
[f] Department of Genetics and Biochemistry, Clemson University, Clemson, South Carolina 29634, United States.
*Corresponding author: rpodila@g.clemson.edu, Phone: 864-656-4447, Fax: 864-656-0805; ssarupr@g.clemson.edu, Phone: 864-656-3258, Fax: 864-656-0784.

the common denominator in their physiological response.[1, 12-15] In case of CNMS, it has been hypothesized that the presence of neutral and charged defects could elicit an adverse physiological response possibly by generating highly reactive oxygen species and inducing structural changes in proteins through charge transfer reactions.[1, 9, 18] Despite this obvious importance of defects and charge transfer in CNM toxicity, the influence of structural and functional defects in CNMs on biomolecular adsorption and immune response remains poorly understood.[21] Although the formation of protein corona on CNMs has been extensively studied in recent years, the underlying physical and chemical processes in protein and defected CNM interactions (e.g., charge transfer between proteins and defects) have not yet been completely understood. To elucidate the role of defects and their associated charge transfer in biological interactions of CNMs, it is imperative to synthesize CNMs with different defect content and study their effects on protein corona.

In this article, we investigated the interaction of bovine serum albumin (BSA) and fibrinogen with defected CNMs such as multi-walled carbon nanotubes (MWNTs), graphene, and graphene oxide nanoribbons (GNRs and GONRs) using micro-Raman spectroscopy, photoluminescence (PL), infrared absorption, electrochemistry and molecular dynamics (MD) simulations. The defects in the CNMs used in this study include edges (e.g., edges coming from finiteness of GNRs), functional groups (e.g., hydroxyl and carboxyl groups on GONRs), and other topological defects (e.g., vacancies and Stone-Wales defects in MWNTs). While MWNTs are seamless cylinders with some topological defects and only a few available edges, GNRs and GONRs provide more edges with different functional groups and are well suited for investigating the influence of defects on protein adsorption. Furthermore, the lack of functional group-type defects on MWNTs makes them more hydrophobic than GNRs (weakly hydrophilic) and GONRs (strongly hydrophilic), allowing us to understand the interplay between shape and defect-induced hydrophilicity of CNMs on their biomolecular interactions. We have identified fibrinogen (tubular structure with high-internal stability) and albumin (globular with relatively low internal stability) as the model proteins of interest due to their contrasting properties and binding affinities. We observed: (i) that BSA exhibited similar adsorption on all the CNMs, whereas fibrinogen showed better binding to GNRs and GONRs, (ii) the charge transfer for the case of BSA (/fibrinogen) adsorbed on MWNTs (/GONR) to be the highest, and (iii) an enhanced relaxation of α-helices in proteins with highest charge transfer/adsorption (viz., MWNTs in case of BSA and GONRs for fibrinogen) suggesting that the charge transfer reactions between proteins and CNMs may be critical to control ENM-biomolecular interactions.

2. Experimental Methods and Materials

2-1 Sample Preparation

In this study, M-grade MWNTs (diameter: 50 nm and length >5 μm) were obtained from NanoTechLabs, Yadkinville, NC. The unzipping and refluxing methods were used to prepare GNRs and GONRs from MWNTs. In the unzipping process, 500 mg of MWNTs were mixed with 100 mL of concentrated H_2SO_4 (Sigma Aldrich, 95-98% purity) and bath-sonicated for 3 hours (Aquasonic P250HT). Subsequently, 2 g of $KMnO_4$ (Sigma Aldrich, >98% purity) was added and stirred for 3 hours at 70 °C. Thereafter 3 mL of 30% H_2O_2 (VWR international, 30% w/w) was added to finish the reaction. The unzipped GNRs were collected by centrifugation (Heraeus Instruments, Labofuge 400, at 2900 rpm for 15 min). The pellet was resuspended 3 times in de-ionized (DI) water and re-centrifuged to remove the residual acid and inorganic salts. All pellets were air dried overnight to remove any remaining impurities. The obtained GNRs were further refluxed with 100 mL 30% H_2O_2 and stirred for 2 hours at 70 °C. After the completion of reflux, 200 mL of concentrated H_2SO_4 (VWR international, 95-98%) was slowly added and the mixture was left to stir for another 1 hour at 70 °C. The resulting suspension was diluted and filtered through 0.45 μm polyamide filter, dried, and resuspended in pure DI water. This procedure was repeated at least 3 times to wash away residual chemicals and obtain GONRs. For the protein binding, BSA (*Spectrum Chemical Mfg. Corp, CA)* and fibrinogen (Alfa Aesar) were incubated at 37 °C for 12 hours with CNMs. We used physiologically relevant concentrations of BSA 5-60 g/L and fibrinogen 0.5-6 g/L. All dilutions for BSA (/fibrinogen) were done in DI water (/0.9 % NaCl). After incubation, suspensions were centrifuged for 15 min at 13,000 rpm (eppendorf minispin) and the obtained pellets were resuspended in DI water. The procedure was repeated at least 3 times to remove any unabsorbed protein.

2-2 Characterization

Transmission electron microscopy (TEM; Hitachi 7600) was performed to investigate changes in CNM structure upon chemical treatment. For TEM, the samples were dispersed in water for 10 mins using 1/8" tip sonicator and the sample was drop casted on a holey carbon (400 mesh; Ted Pella) and was dried overnight. Contact angle measurements were performed on freestanding CNM buckypapers using a custom-built setup equipped with Celestron's 44302 digital USB microscope. We prepared freestanding buckypapers for all different types of CNMs by vacuum filtering CNM suspensions in water (1 mg/ml, sonicated using 1/8" tip sonicator for 30 minutes) through a 0.45 mm nylon filter paper. Subsequent to filtration, the CNM materials were peeled off from the filter paper by heat treating the samples at 60 ^{o}C overnight. All the Raman spectra were obtained on dry powders using a 514.5 nm Ar^{+} excitation coupled to a Renishaw InVia micro-Raman spectrometer.

PL spectra was measured at 280 nm excitation wavelength and 300-450 nm emission range with 5 nm slit width using a Horiba iHR 550 spectrometer equipped with a TRIAX 550 liquid N_2 cooled CCD. For the PL measurements, 3 ml of CNM-protein suspension was used in a 10 mm wide quartz cuvette. Fourier Transform Infrared (FTIR) spectroscopy was performed on a Thermo Scientific Nicolet 6700 ATR-FTIR and Bruker IFS 66v/S. For FTIR measurements, the samples were drop casted onto a monolithic diamond crystal and the signal from DI water was used as the background.

Cyclic voltammetry was carried out to measure the charge transfer properties between the MWNTs and proteins solutions. The experiments were performed with a Reference 3000 Potentiostats electrochemical measurement system (Gamry Instruments, Inc.). A platinum mesh was used as the counter electrode and Ag/AgCl as the reference electrode. The electrolyte solution consisted 40 g/L of BSA or 4 g/L of fibrinogen. All the data was obtained at a low scan rate (5 mV/s) to avoid any diffusion limitations.

2-3 Molecular Dynamics Simulation

We performed large-scale MD simulations of BSA (4F5S.pdb)[22] in explicit water in the presence of two different CNMs – GNR and GONR. The surface area of both the CNMs was kept the same in the simulations. GONR was generated using the methodology described in DeFever *et al* [23] and was 30% oxidized. The Amberff99SB-ILDN force field was used to describe the protein and GNR.[24] TIP3P model was used for water.[25] GONR was described using the OPLS force field[24] because this eliminates the necessity of determining the partial charges on the GONR atoms using ab initio calculations.

The simulation systems comprised of the CNM, 9220 protein atoms and approximately 70,000 water molecules. Ions were added to neutralize the system. To enhance the sampling of protein adsorption in the MD simulations we performed 10 simulations for each system. In these 10 simulations, we used 10 different protein orientations in the starting configurations. This enabled us to sample different regions of the protein that could adsorb to the CNMs. We note that this does not capture all the regions of the protein that could adsorb to the CNMs and also does not specify the affinity of various regions to the CNMs – neither of which are the goals of these simulations. The protein was placed at a distance such that no two heavy atoms of the protein and CNM were closer than 8 Å in the starting configurations of the simulation. Each simulation was run for 100 ns, resulting in effectively 1 μs (10 orientations x 100 ns) simulation per CNM-BSA-water system.

The long-range electrostatic interactions were calculated using PME as implemented in GROMACS v5.0.2.[26] The velocity-rescaling thermostat[27] and Berendsen barostat[28] were used to maintain the temperature at 300 K and pressure at 1 bar, respectively. The bonds involving hydrogen atoms were constrained using LINCS algorithm.[29] The time step used was 2 fs. The simulations were performed on 20 CPUs + 2 K20 GPUs and each 100 ns long simulation took ~6 days to complete. Configurations were stored every 20 ps for further analysis.

3. Results and Discussions

3-1 Electron Microscopy and Raman Spectroscopy:

As shown in Figs. 1 a-c, we synthesized GNRs and GONRs by unzipping and subsequently oxidizing pristine MWNTs. FTIR measurements (see supplementary information Fig. S1) revealed the absence of functional group-type defects on MWNTs, while showed the presence of hydroxyl groups on GNRs, which possibly formed on the edges of unzipped MWNTs during chemical reflux and the unzipping process. In contrast to MWNTs and GNRs, GONRs exhibited more functional groups such as epoxide, hydroxyl, and carboxyl

functionalities (see Fig. S1). The presence of polar functional groups on GNRs and GONRs indicate that they are more hydrophilic than MWNTs and could be ranked as MWNTs > GNRs > GONRs in terms of hydrophobicity. Concurrent with the observations from FTIR, our contact angle measurements confirmed the non-wettable nature of MWNTs and GNRs (Fig. S2). As expected from the presence of polar groups on GONRs, water was found to wet GONRs confirming the hydrophilic nature.

The Raman spectra of all CNMs used in this study (Fig. 2) showed the graphitic band (or G-band), arising from longitudinal and transverse optical phonons ~1585 cm^{-1}, along with the so-called disorder or D-band at 1350 cm^{-1}. The integrated intensity of the D-band to that of the G-band (I_D/I_G ratio) is often used as a measure of average defect-defect spacing in CNMs.[30] Clearly, as seen from Fig. 2, the I_D/I_G ratio is higher for GONR and GNRs than the pristine MWNTs, which could be attributed to the harsh chemical reactions in the unzipping and oxidation processes. While GNRs are unzipped through only one-time exposure to sulphuric acid and $KMnO_4$, GONRs undergo a two-step chemical process (i.e., unzipping and subsequent oxidation) leading to an increased D-band intensity in their Raman spectrum. Furthermore, the overtone of D-band (called 2D-band ~2700 cm^{-1}) was found to significantly decrease in intensity (at least by 10 times, as shown in Fig. 2 inset) in GONRs due to oxidation. The full-width at half-maximum of G-band in GNRs (~28 cm^{-1}) and GONRs (~40 cm^{-1}) also increased significantly relative to pristine MWNTs (~20 cm^{-1}) indicating a decrease in phonon lifetime due to the presence of different type of defects (particularly, edges and functional group-type defects in GNRs and GONRs). Additionally, a defect-induced Raman feature ~1620 cm^{-1}, often activated at high defect concentrations, is clearly observed for both GNRs and GONRs. Juxtaposing Raman, FTIR, and contact angle measurements, it could be concluded that MWNTs are less-defective (I_D/I_G ~0.35) and more hydrophobic (no presence of functional groups), while GNRs (/GONRs) are slightly (/highly) defective (I_D/I_G ~0.83 for GNRs and 0.94 for GONRs) and weakly (/strongly) hydrophilic due to the presence of polar functional groups.

3-2 Adsorption isotherms:

The protein adsorption on different CNMs was characterized using adsorption isotherms obtained through photoluminescence studies. Previously, we showed that the intrinsic emission of proteins (~345 nm upon 280 nm excitation) from aromatic amino acids such as tryptophan, tyrosine and phenylalanine could be used to quantify the unknown concentration of a protein through the use of a standard curve.[9] We obtained a standard calibration curves for BSA and fibrinogen (see Fig. S3) by measuring their intrinsic photoluminescence at various concentrations in an aqueous medium. Subsequently, the adsorption isotherms for BSA and fibrinogen on CNMs were obtained by measuring the PL signal from adsorbed proteins and acquiring the protein concentration from the standard curves in Fig. S3. Although the shape of experimental isotherms for protein adsorption often appears strikingly similar to the Langmuir isotherm, the use of the Langmuir isotherm is inappropriate in our case because of its assumptions such as: i) the equivalence of all adsorption sites, ii) one-to-one binding between each adsorption site and the adsorbed molecules, iii) the absence of interaction between adsorbed solutes, and iv) the dynamic reversibility of the adsorption process.[31] In reality, adsorbed proteins tend to rapidly undergo surface-induced unfolding and reorientation to increase their contact area to irreversibly stick to the material surface.

As shown in Fig. 3, the adsorption of BSA and fibrinogen on CNMs was observed to follow a Freundlich isotherm. Unlike Langmuir model, the Freundlich isotherm is more appropriate to describe the adsorption processes, as it does not assume uniformity, one-to-one binding, and the absence of protein-protein interactions. The Freundlich adsorption isotherm is mathematically expressed as:

$$\log a = (1/n) log\ C + \log K \quad (1),$$

where α is the amount of adsorbed protein, C is the initial concentration of adsorbed protein; $1/n$ and K are constants that indicate the intensity and capacity of adsorption, respectively. We obtained the $1/n$ and K values (see Table 1) for BSA and fibrinogen adsorption on various CNMs by fitting the data in Fig. 3.

We observed that $1/n$ and K values are similar for the adsorption of BSA on all CNMs (Table 1). In the case of MWNTs (hydrophobic) and GNRs (which are only weakly hydrophilic), a "shell" of interacting water molecules plausibly forms around the hydrophobic surface decreasing the entropy. The disruption of this shell upon protein adsorption is more energetically favourable because the release of otherwise constrained water molecules leads to an increase in the entropy. Additionally, the energy

of BSA-MWNT/GNR system could be reduced by the relaxation of protein secondary structures to increase the protein entropy. Thus, the adsorption of BSA on to MWNTs and GNRs could be expected to increase with increasing protein concentration (Fig. 3). The low 1/*n* values (*cf.* Table 1) for GONRs showed that GONR exhibited relatively weaker interaction with BSA. Surprisingly, the difference in 1/*n* values for the adsorption of BSA on GONRs was only slightly different from MWNTs and GNRs despite their hydrophilicity. The hydrophilic nature of GONRs does not constrain water molecules, unlike MWNTs and GNRs, and thus the adsorption of BSA on GONRs is not accompanied by significant entropy increase from the release of water molecules. Nevertheless, a comparable 1/*n* value for the adsorption of BSA on GONRs could be attributed to the formation of energetically favorable hydrogen bonds between BSA and functional group-type defects on GONRs (particularly, hydroxyl and carboxyl groups shown in Fig. S1).

3-3 Molecular Dynamics Simulations:

To further understand these unexpected CNM-BSA interactions, we performed large-scale molecular dynamics (MD) simulations of BSA-GNR/GONR-water systems. As shown in Figs. 4a and b, we observed a decrease in the BSA-GNR/GONR interaction energy indicating that BSA associates with GNRs and GONRs consistent with our experiments. Furthermore, the adsorption process was found to occur in steps (as seen in the series of plateaus and steep drops in Figs. 4a and b) primarily because BSA undergoes conformational changes after initial contact (in accordance with our experimental observations, discussed later in Fig. 5) leading to some protein regions collapsing on to the CNM surface rather than gradually spreading from the initial region of contact.[32] In the case of GNRs, most simulations resulted in interaction energies < -380 kJ/mol within 100 ns of the simulation unlike BSA-GONR-water simulations. This suggests that BSA displays more affinity to GNR compared to GONR, consistent with the experimental findings that BSA prefers more hydrophobic surfaces (as seen by higher 1/*n* values for adsorption of BSA on GNR compared to GONR in Table 1). We observed that water molecules are released from the hydration shells of BSA, GNR and GONR as BSA adsorbs to the CNMs (Figs. 4c and d). The total number of water molecules in the hydration shell of the protein and GNR is lower (i.e., the number of released water molecules is higer) than that in the case of the BSA-GONR system. As discussed before (cf. Fig. 3), such a result is expected because relatively more water molecules interact with GONR due to its hydrophilicity. Nonetheless, in both cases of GNRs and GONRs, BSA adsorbs well on to the CNM due to favourable interaction energy and a decrease in the total number of water molecules in the hydration shell of the BSA-CNM complex.

Returning to Fig. 3, in case of fibrinogen, 1/*n* and *K* values for MWNTs were found to be lower when compared to GNRs and GONRs. It may be rationalized that fibrinogen, which is a hard protein due to its excellent internal stability, has a lower tendency than BSA (a soft protein) to relax its secondary structure for adsorbing on to a tubular structure as in the case of MWNTs. GNRs and GONRs, unlike MWNTs, provide a flat-sheet like structure (*cf.* Fig. 1) which is more energetically favourable for the adsorption of fibrinogen even without unfolding. Furthermore, similar to the case of BSA, it could be expected that the functional groups on GONRs facilitate hydrogen bonds with fibrinogen.

3-4 FTIR studies on secondary structure changes:

In the formation of the protein corona, the protein molecules initially adsorb on to the CNMs while largely retaining their native-state structure. Subsequently, the adsorbed protein can begin to relax its secondary structure, unfold, and spread out on the CNM surface and transition from an end-on to a side-on orientation.[33, 34] The degree of protein unfolding on a surface is influenced by the strength of the protein-surface interactions relative to the internal stability of the protein.[35-37] Accordingly, to elucidate the adsorption-induced structural changes in proteins, we obtained the FTIR spectra of adsorbed proteins as shown in Fig. 5. It should be noted that CNMs exhibit strong absorption <240 nm due to their π-electron system precluding the use of traditional tools such as circular dichroism for the evaluation of protein secondary structure. As evident from Figs. 5a and b, the α-helical content in BSA leads to strong adsorption ~1640-1660 cm^{-1} (shown in dashed lines) while the lower frequency component at ~1620-1640 cm^{-1} and the peak ~1555 cm^{-1} arise from β-sheets.[36,37] Clearly, the rich secondary structure of BSA (particularly, the peak relating to α-helical content) significantly disappears upon its adsorption on to all CNMs, as expected from its low internal stability. Indeed, the changes in secondary structure are higher in the case of MWNTs (i.e., complete disappearance of secondary structure) suggesting that BSA unfolds much more, relative to GNRs and GONRs, in order to adhere to the tubular

MWNTs. GNR and GONR retain BSA secondary structure to certain extent, as shown by the presence of ~1555 cm^{-1} for β-sheets. In the case of fibrinogen, the secondary structural changes are found to be higher for GONRs compared to MWNTs and GNRs plausibly due to the formation of hydrogen bonds. The α-helix peak was found to partially disappear for fibrinogen adsorbed on MWNTs and GNRs. Lastly, the structural changes for fibrinogen on GNRs seemed to be less pronounced than MWNTs possibly due to its shape. It could be rationalized that fibrinogen must unfold more to adhere to MWNTs due to their higher curvature than GNRs.

3-5 Cyclic Voltammetry:

The chemisorption of proteins on bulk material surfaces has been known to occur through charge transfer processes.[34, 38-40] It may be expected that a surface facilitating higher charge transfer at the nanoscale may lead to stronger surface-protein interactions and a subsequent increase in protein adsorption. To validate such a hypothesis, we performed cyclic voltammetry (CV) measurements with CNMs as a working electrode in protein electrolyte solution (Fig. 6). In CV characterization, the application of gate voltage on the working electrode modulates its electronic energy levels, which when above (/below) the LUMO (/HOMO) levels of the protein can result in a charge transfer. Although the proximity of electronic levels make charge transfer between protein in electrolyte solution and the working electrode (i.e., CNMs) thermodynamically favourable, the probability of charge transfer depends upon density of electronic states at the Fermi level (DOS(E_F)) in the working electrode (CNMs in this case). In defect-free CNMs (e.g., perfect sheet of graphene with no defects), the DOS(E_F) is very low (almost zero for graphene) and therefore charge transfer is often not observable in the experiments.[9,41] However, in our case, the presence of defects (introduced through unzipping in GNRs and oxidation in GONRs) induces new electronic states in CNMs which could increase the DOS(E_F), and thereby lead to strong interactions between the protein and CNMs through charge transfer. In a typical CV plot, a peak in current (in a current vs. voltage plot such as the one shown in Fig. 6) indicates the presence of charge transfer between the electrolyte (i.e., protein solution in our case) and the working electrode (i.e., CNMs). Interestingly, the amount of charge transfer (Fig. 6) does not concomitantly increase with increasing I_D/I_G (cf. Fig. 2). Such an observation may be rationalized by the fact that the electronic structure (i.e., both energy levels and DOS(E_F)), which is dependent on shape, size, and defect density of CNMs, is different for MWNTs, GNRs, and GONRs. Nonetheless, in the case of BSA (/fibrinogen), the charge transfer was found to be the highest for MWNTs (/GONRs), which exhibited highest secondary structural changes (*cf.* Fig. 5) for BSA (/fibrinogen) suggesting that charge-transfer may induce protein unfolding or vice versa.

When taken together, photoluminescence, Raman, infrared, and electrochemistry measurements suggest that: i) the defect-induced hydrophilicity can alter the formation of protein corona in CNMs, and ii) the net charge transfer between protein and CNM and the change in secondary structures may be correlated, indicating that protein corona formation is accompanied by both charge-transfer and protein unfolding.

4. Conclusions

In summary, we investigated the binding of bovine serum albumin (BSA) and fibrinogen with different carbon nanomaterials. Raman spectroscopy measurements showed a higher amount of defects in graphene and graphene oxide nanoribbons (GNRs and GONRs) compared to pristine multi-walled nanotubes (MWNTs). The binding experiments showed that the BSA adsorbs equally on all MWNTs, GNRs, and GONRs while fibrinogen showed a significantly lower adsorption on MWNTs. The lower adsorption of fibrinogen on MWNTs was attributed to its hardness relative to BSA. Furthermore, it is observed that the net conformational changes (gleaned from infrared spectroscopy) in protein structure were highest for the cases of highest charge transfer (observed in cyclic voltammetry) between protein and CNMs. Our results show that the formation of protein corona is sensitive to the defects on CNMs and is accompanied by both charge-transfer and protein unfolding.

Acknowledgements

J.B. and R.P. gratefully acknowledge funding support from NIH NIEHS R03- ES023036. R. P. and S.S. acknowledge their Clemson University Start-Up funds and resources from Palmetto Supercomputer maintained by Clemson Computing and Information Technology group. R. P and A. M. R thank Aleksandr Kakinen, Estonia for his initial contributions to the project.

References

1 R. Podila, J.M. Brown, *Journal of Biochemical and Molecular Toxicology,* 2013, **27(1)**, 50-5.
2 P Wick, M.J.D. Clift, M. Roesslein, B Rothen-Rutishauser, *Chemsuschem*., 2011, **4(7)**:905-11.
3 J.H. Shannahan, X. Lai, P.C. Ke, R. Podila, J.M. Brown, F.A. Witzmann, *Plos One,* 2013;**8(9)**, e74001.
4 T. Cedervall, I. Lynch, S. Lindman, T. Berggard, E. Thulin, H. Nilsson, K.A. Dawson, S. Linse, *Proceedings of the National Academy of Sciences of the United States of America*, 2007, **104(7)**, 2050-5.
5 A.E. Nel, L. Maedler, D. Velegol, T. Xia, E.M.V. Hoek, P. Somasundaran, F. Klaessig, V. Castranova, M. Thompson, *Nature Materials,* 2009, **8(7),** 543-57.
6 I. Lynch, K.A. Dawson, *Nano Today,* 2008, **3(1-2)**, 40-7.
7 D. Walczyk, F.B. Bombelli, M.P. Monopoli, I. Lynch, K.A. Dawson, *Journal of the American Chemical Society*, 2010, **132(16)**, 5761-8.
8 R. Podila, R. Chen, P.C. Ke, J.M. Brown, A.M. Rao, *Applied Physics Letters*, 2012, **101(26)**, 263701.
9 R. Podila, P. Vedantam, P.C. Ke, J.M. Brown, A.M. Rao, *Journal of Physical Chemistry C*, 2012, **116(41)**, 22098-103.
10 A.A. Aldossari, J.H. Shannahana, R. Podila, J.M. Brown, *Toxicology in Vitro*, 2015, **29(1)**, 195-203.
11 J.H. Shannahan, R. Podila, A.A. Aldossari, H. Emerson, B.A. Powell, P.C. Ke, A.M. Rao, J.M. Brown, *Toxicological science: an official journal of the Society of Toxicology*, 2015, **143(1)**, 136-46.
12 R. Landsiedel, L. Ma-Hock, A. Kroll, D. Hahn, J. Schnekenburger, K. Wiench, W. Wohlleben, *Advanced Materials*, 2010, **22(24)**, 2601-27.
13 F. Watari, N. Takashi, A. Yokoyama, M. Uo, T. Akasaka, Y. Sato, S. Abe, Y. Totsuka, K. Tohji, *Journal of the Royal Society Interface*, 2009, **6**, S371-S88.
14 B. Fubini, I. Fenoglio, M. Tomatis, F. Turci., *Nanomedicine,* 2011, **6(5)**, 899-920.
15 X. Zhu, Y. Chang, Y. Chen, *Chemosphere*, 2010, **78(3)**, 209-15.
16 Z. Yang, Z. Wang, X. Tian, P. Xiu, R. Zhou, *Journal of Chemical Physics,* 2012, **136(2)**, 025103.
17 R. Haddad, S. Cosnier, A. Maaref, M. Holzinger, *Analyst*, 2009, **134(12)**, 2412-8.
18 C.P. Firme III, P.R. Bandaru, *Nanomedicine-Nanotechnology Biology and Medicine*, 2010, **6(2)**, 245-56.
19 K. Bradley, M. Briman, A. Star, G. Grüner, *Nano Letters*, 2004, **4(2)**, 253-256.
20 C. N. R. Rao, R. Voggu, *Materials Today*, 2010, **13(9)**, 34-40.
21 R. Podila, J.M. Brown, A. Kahru, A.M. Rao, *MRS Bulletin*, 2014, **39(11)**, 990-995.
22 A. Bujacz, *Acta Crystallographica Section D: Biological Crystallography*, 2012, **68(10)**, 1278-1289.
23 R. S. DeFever, N. K. Geitner, P. Bhattacharya, F. Ding, P. C. Ke, S. Sarupria, *Environmental science & technology*, 2015, **49(7)**, 4490-4497.
24 K. Lindorff-Larsen, S. Piana, K. Palmo, P. Maragakis, J. L. Klepeis, R. O. Dror, D. E. Shaw, *Proteins: Structure, Function, and Bioinformatics*, 2010, **78(8)**, 1950-1958.
25 W. L. Jorgensen, J. Chandrasekhar, J. D. Madura, R. W. Impey, M. L. Klein, *The Journal of chemical physics*, 1983, **79(2)**, 926-935.
26 B. Hess, C. Kutzner, D. Van Der Spoel, E. Lindahl, *Journal of chemical theory and computation*, 2008, **4(3)**, 435-447.
27 G. Bussi, D. Donadio, M. Parrinello, *The Journal of chemical physics*, 2007, **126(1)**, 014101.
28 H. J. Berendsen, J. P. M. Postma, W. F. van Gunsteren, A. R. H. J. DiNola, J. R. Haak, *The Journal of chemical physics*, 1984, **81(8)**, 3684-3690.
29 B. Hess, H. Bekker, H. J. Berendsen, J. G. Fraaije, *Journal of computational chemistry*, 1997, **18(12)**, 1463-1472.
30 L. M. Malard, M. A. Pimenta, G. Dresselhaus, M. S. Dresselhaus, *Physics Reports*, 2009, **473(5)**, 51-87.
31 R.A. Latour, *Journal of Biomedical Materials Research Part A*, 2015, **103(3)**, 949-58.
32 J. W. Shen, T. Wu, Q. Wang, Y. Kang, *Biomaterials*, 2008, **29(28)**, 3847-3855.
33 C.M. Alves, R.L. Reis, J.A. Hunt, *Journal of the Royal Society Interface*, 2010, **7(50)**, 1367-77.
34 M. Rabe, D. Verdes, S. Seeger, *Advances in Colloid and Interface Science*, 2011, **162(1-2)**, 87-106.
35 S. Gupta, M. Camargo, J. Stellbrink, J. Allgaier, A. Radulescu, P. Lindner, E. Zaccarelli, C. N. Likos. D. Richter, *Nanoscale*, 2015, **7(33)**, 13924-13934.
36 M. Jackson, H.H. Mantsch, *Critical Reviews in Biochemistry and Molecular Biology,* 1995, **30(2)**, 95-120.
37 J. Kong, S. Yu, *Acta Biochimica et Biophysica Sinica* 2007, **39(8),** 549–559
38 W. Norde, *Croatica Chemica Acta*, 1983, **56(4)**, 705-20.
39 N.R. Cabilio, S. Omanovic, S.G. Roscoe, *Langmuir*, 2000, **16(22)**, 8480-8.
40 A. Carre, *Journal of Adhesion Science and Technology*, 2010, **24(5)**, 813-4.
41 R. Podila, T. Moore, F. Alexis, and A.M. Rao, *RSC Advances*, 2013, **3 (6)**, 1660-1665.

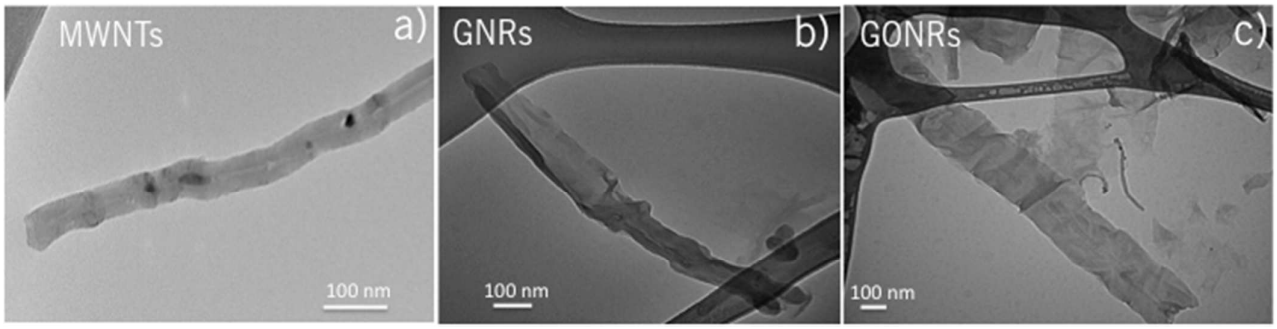

Figure 1: Transmission electron microscope images of multi-walled carbon nanotubes (MWNTs) (a), graphene nanoribbons (GNRs) (b), and graphene oxide nanoribbons (GONRs) (c). The scale bars are 100 nm.

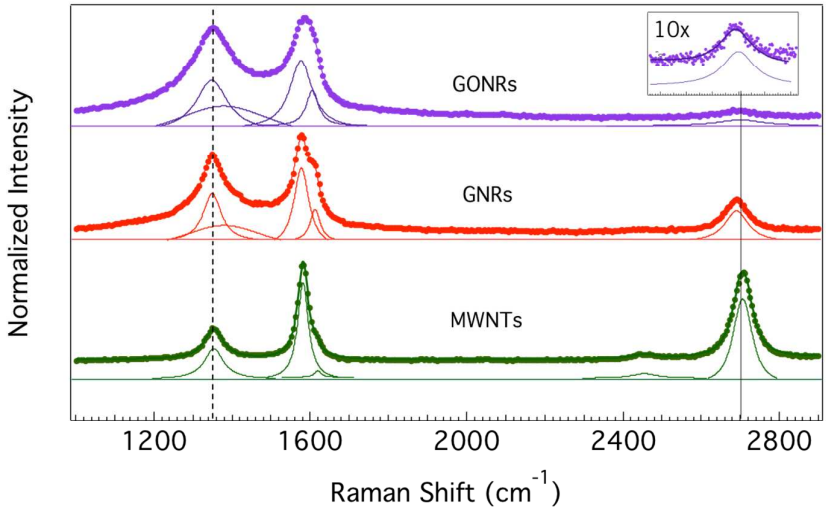

Figure 2. Raman spectra for pristine MWNTs, GNRs, and GONRs show the graphitic (G-band) at ~1585 cm^{-1}. The defect band (D-band ~1350 cm^{-1}; indicated by the dotted line) to G-band ratio (I_D/I_G) is high for GONRs (~0.94) compared to GNRs (~0.84) and MWNTs (~0.35) due to the harsh chemical treatment used in the two-step oxidation process. The 2D-band ~2700 cm^{-1} (indicated by a solid line) is significantly lower for GNRs and GONRs relative to MWNTs due lattice disruption induced by chemical treatment. The dots show experimental data and lines represent theoretical fits obtained from convolution of Lorentzian peaks shown below each spectrum. The inset shows a magnified 2D band in GONRs, which is at least 10 times weaker relative to MWNTs due to oxidation.

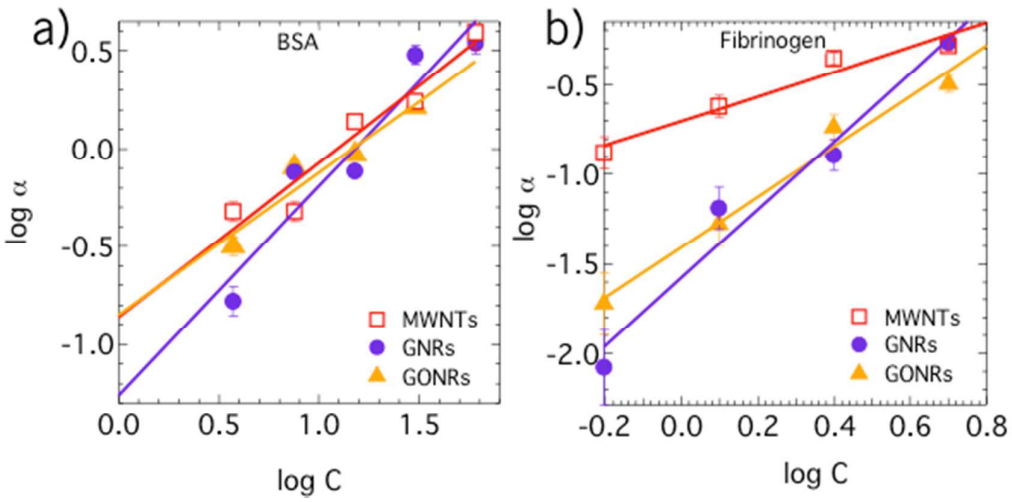

Figure 3. Adsorption isotherms for BSA (a) and fibrinogen (b) on to various carbon nanomaterials (CNMs) obtained using the intrinsic photoluminescence of aromatic acids in BSA and fibrinogen. The trends match a Freundlich isotherm model suggesting non-uniform and multivalent adsorption sites on carbon nanomaterials. BSA exhibits similar adsorption on all CNMs with slightly lower adsorption on GONRs (cf. Table 1). Fibrinogen exhibits a relatively strong adsorption of GNRs and GONRs, relative to MWNTs, possibly due to their flat-sheet like structure.

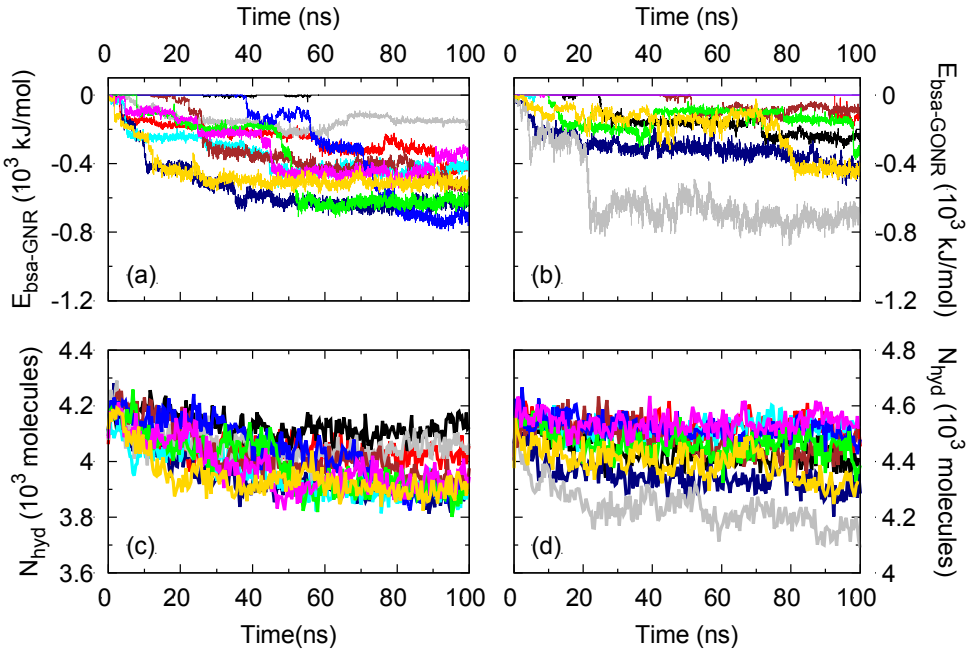

Figure 4. Interaction energy of BSA with (a) GNR and (b) GONR during the molecular dynamics simulation. Number of water molecules in the hydration shell (N_{hyd}) of (c) BSA-GNR and (d) BSA-GONR during the course of the simulation. N_{hyd} was calculated as the number of water molecules within 5 Å of the protein or CNM heavy atoms. Each color represents data from one simulation and results from all the 10 independent simulation runs are shown. Notice that N_{hyd} is lower for BSA-GNR (compared to BSA-GONR system) as more water molecules are released from GNR due to its stronger hydrophobic character.

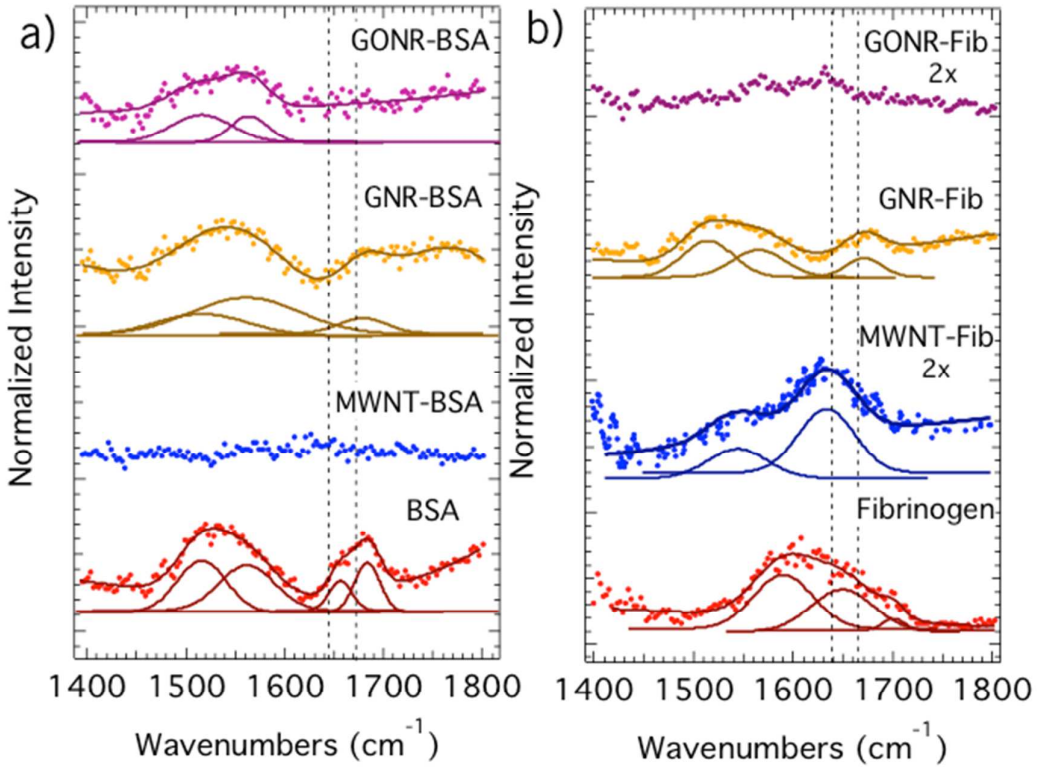

Figure 5. (a) FTIR spectra for native BSA, BSA-adsorbed on MWNTs, GNRs, and GONRs show that the CNMs significantly affected the secondary structures of the proteins. The absorption peak for α-helix in native BSA, in the range from 1640 to 1660 cm^{-1} (indicated by the vertical dashed lines), showed a significant reduction (disappeared for MWNTs) for all CNMs suggesting that the secondary structure of BSA adsorbed on CNMs was less compact. (b) In the case of fibrinogen, the loss of secondary structure was highest for GONRs possibly due to the formation of hydrogen bonds. While both MWNTs and GNRs exhibited a loss of α-helical content, the appearance of new peak ~1500 cm^{-1} (corresponding to random secondary structure motifs) in GNRs suggested a lesser degree of relaxation for fibrinogen, compared to MWNTs.

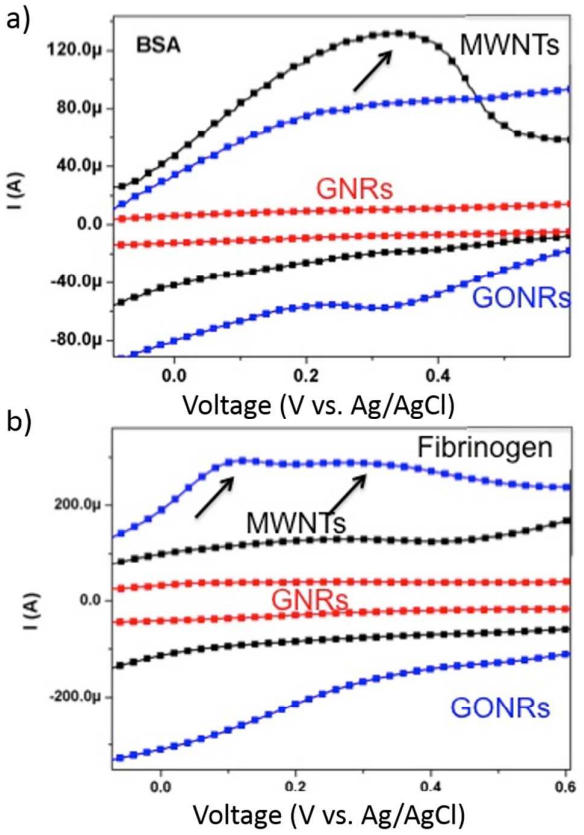

Figure 6. Cyclic voltammograms for BSA (a) and fibrinogen (b) protein solutions on carbon nanomaterial material working electrodes. MWNTs (/GONRs) exhibit a broad peak(s) (indicated by a solid arrow) with BSA (/fibrinogen) indicative of an irreversible redox reaction suggesting a charge transfer.

Nanomaterial	*1/n*		*K*	
	BSA	Fibrinogen	BSA	Fibrinogen
MWNTs	0.79	0.68	0.42	0.49
GNR	0.9	1.9	0.30	0.2
GONR	0.73	1.4	0.42	0.24

Table 1: Freundlich isotherm parameters for the adsorption of BSA and fibrinogen on different carbon nanomaterials.

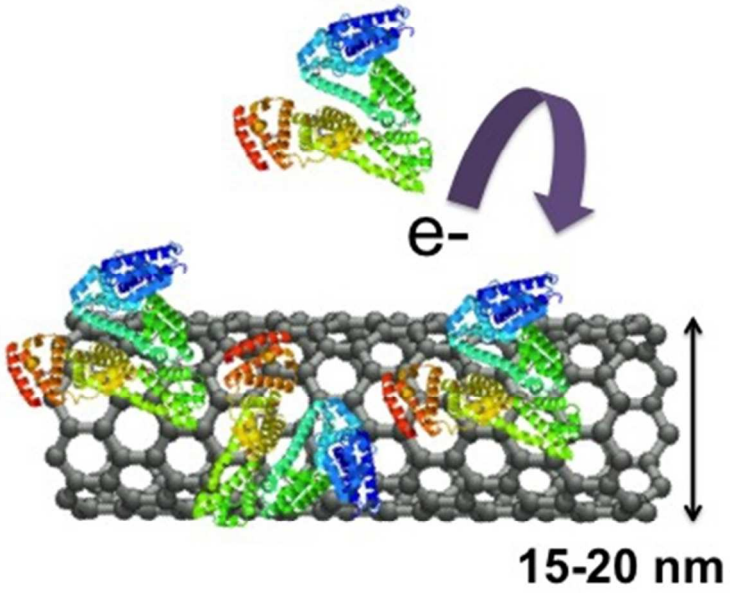

143x152mm (72 x 72 DPI)